ACS APPLIED MATERIALS & INTERFACES

Research Article

www.acsami.org

Controlling Available Active Sites of Pt-Loaded TiO_2 Nanotube-Imprinted Ti Plates for Efficient Dye-Sensitized Solar Cells

Lu-Yin Lin,*[,§,ϕ] Min-Hsin Yeh,[†,ϕ] Wei-Chieh Chen,[†] Vittal Ramamurthy,*[,†] and Kuo-Chuan Ho*[,†]

[†]Department of Chemical Engineering, National Taiwan University, Taipei 10617, Taiwan

[§]Department of Chemical Engineering and Biotechnology, National Taipei University of Technology (Taipei Tech), Taipei 10608, Taiwan

Supporting Information

ABSTRACT: The counter electrode (CE) of dye-sensitized solar cells (DSSCs) plays an important role for transferring electrons and catalyzing the I^-/I_3^- reduction. Active surface area of the substrate determines the reduction sites of the deposited catalyst as well as the catalytic ability of the CE. An effective method for enhancing and controlling the active surface area of metal plates is provided in this study. The Ti plates are imprinted by TiO_2 nanotubes (TNT) via the technique of anodization along with the ultrasonic vibration process. The available active area of imprinted Ti plates is controlled by varying the anodization voltage to produce TNT imprints with different diameters and depths. A solar-to-electricity conversion efficiency (η) of 9.35% was obtained for the DSSC with a TNT-imprinted Ti plate as the CE substrate, while the cell with an imprint-free Ti plate shows an η of 7.81%. The enhanced η is due to the improved electrocatalytic ability of the CE by using the TNT-imprinted Ti plate as the substrate with higher active surface area.

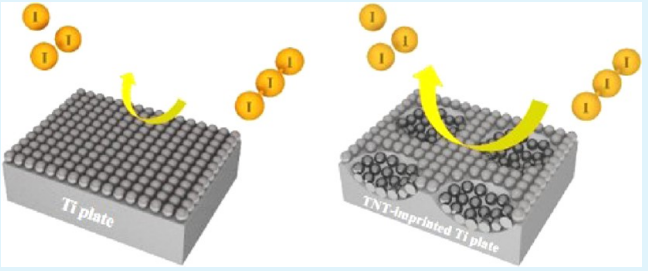

KEYWORDS: *anodization, cyclic voltammetry, counter electrode, dye-sensitized solar cell, titanium dioxide nanotubes, titanium plate*

INTRODUCTION

The counter electrode (CE) of dye-sensitized solar cells (DSSCs) is a key component for transferring electrons from the external circuit and catalyzing the redox reaction in the electrolyte. High electrical conductivity, good electrocatalytic ability, and excellent corrosion resistance are indispensable properties for the CE.[1−6] Pt is widely used as the catalytic layer due to its superior electrocatalytic activity for the I^-/I_3^- redox reaction.[7−11] Transparent conducting oxide (TCO) glasses are conventionally used as the substrate for DSSCs,[12,13] but its fragile and inflexible properties limits the application. In consideration of this, flexible metal plates with excellent electrical and thermal conductivities are an alternative choice.[14,15] Using inexpensive metals as the substrate of DSSCs not only reduces the fabrication cost and the internal resistance of the cell but also provides good heat radiation property.[16−19] Miettunen et al. reported that a DSSC with a Ti plate as the CE substrate remained stable under 1000 h of light soaking.[20] Wang et al. concluded that a Pt-coated Ti plate acted better than a Pt-coated fluorine-doped SnO_2 (FTO) conducting glass as the CE of DSSCs due to the lower sheet resistance and higher light reflectance for the former case.[21] To improve the electrocatalytic ability of the CE, many researchers focused on increasing the catalyst active surface area by modifying its structure and properties,[22,23] but there are just few reports devoted to enhance the surface area of the substrate deposited by the catalyst. Fu et al. proposed a photoplatinization technique to deposit Pt on a thin TiO_2 layer modified plastic substrate at low temperature as the counter electrode for flexible DSSCs and got an η of 6.97%.[24] Kim et al. used a facile process to produce large-area Pt counter electrode platforms with well-arrayed, mesh-shaped nanopatterns and obtained a high η of 7.0% for solid-state DSSCs.[25] Hasin and co-workers made a CE of DSSCs by impregnating Pt nanoparticles in a mesoporous Nb-doped TiO_2 film. The Pt/Nb-doped TiO_2 film shows a reduced charge transfer resistance and an increased exchange current density due to the large active surface area of the mesoporous Nb-doped TiO_2 substrate for Pt deposition.[26] Our group applied a composite poly(3,3-diethyl-3,4-dihydro-2*H*-thieno-[3,4-*b*][1,4]-dioxepine)/Pt (PProDOT-Et_2/Pt) film as the catalyst layer on the CE of DSSCs to provide higher active surface area for Pt loading by the PProDOT-Et_2 nanonet.[27] Tang et al. prepared a one-dimensional polyaniline (PANI) nanofiber film to provide more sites for Pt deposition.[28]

In this study, an effective method was applied to fabricate Ti plates with high active surface area in a controllable fashion, and the as-prepared Ti plates were loaded with platinum and applied as the CE of DSSCs. Ti plates were first anodized at various voltages to form TiO_2 nanotubes (TNTs) on the surface, and the TNTs were removed completely by vibrating ultrasonically in the deionized water (DI-water) subsequently.

Received: July 31, 2014
Accepted: February 2, 2015
Published: February 2, 2015

© 2015 American Chemical Society

DOI: 10.1021/am505025e
ACS Appl. Mater. Interfaces 2015, 7, 3910−3919

Consequently, only TNT imprints remained on the Ti plate surface. In fact, an easier method was proposed to enhance the active surface area of metal substrates by acid treatment. Yun et al. roughened stainless steel plates electrochemically using a sulfuric acid solution containing the hydrated sodium thiosulfate and the propargyl alcohol.[29] Yun et al. also reported that the acid treatment on Ti substrates significantly improves the electrical and optical behaviors.[30] However, the active surface area is hard to control and thus is not easily reproduced with the acid treatment. Moreover, acid treatment would lead to unnecessary formation of metal oxides and an increase in the electrical resistance of metal substrates. On the other hand, in the view of large scale mass production, the uniformity of the substrate is very important. Uniform surface morphology and roughness of the Ti substrates over large surface area can be achieved via the TNT imprinting method provided in this study, while high active surface area with controllable fashion cannot be obtained by simply treating the Ti substrate with the acid. X-ray diffraction (XRD) technique was applied to confirm the formation of TNT imprints. Scanning electron microscopy (SEM) and atomic force microscopy (AFM) were employed to characterize the morphology of Ti plates. The electrocatalytic abilities of the Pt-loaded Ti plates with TNT imprints obtained at various anodized voltages were compared. The DSSC with Pt-loaded Ti plates with TNT imprints as the CE showed an η of 9.35%, with respect to that of the DSSC with a Pt-loaded imprint-free Ti plate as the CE (7.81%). Cyclic voltammetry (CV), electrochemical impedance spectroscopy (EIS), Tafel plots, and incident photon-to-current conversion efficiency (IPCE) spectra were employed to substantiate the explanations.

EXPERIMENTAL SECTION

Materials. Lithium iodide (LiI, synthetical grade), iodine (I_2, synthetical grade), and poly(ethylene glycol) (PEG, M.W. ≈ 20 000 g mol^{-1}) were obtained from Merck. 4-tert-butylpyridine (TBP, 96%) and *tert*-butyl alcohol (tBA, 96%) were obtained from Acros. Titanium tetraisopropoxide (TTIP, > 98%), 2-methoxyethanol (≥99.5%), neutral cleaner, lithium perchlorate ($LiClO_4$, ≥ 98.0%), isopropyl alcohol (IPA, 99.5%), and H_2SO_4 (ACS reagent, 98.0%) were purchased from Aldrich. 3-methoxypropionitrile (MPN, 99%) was received from Fluka. Acetonitrile (ACN) (99.99%) and ammonium fluoride (NH_4F, ACS reagent, 99.2%) were procured from J. T. Baker. 1,2-dimethyl-3-propylimidazolium iodide (DMPII, > 99.5%) was bought from Solaronix. Ethylene glycol (EG, extra pure) was acquired from Scharlau. The organic solvent electrolyte used in this study contains a mixture of 0.1 M LiI, 0.6 M DMPII, 0.05 M I_2, and 0.5 M TBP in a solvent of MPN and ACN (volume ratio of 1:1).

Preparation and Characterization of the Photoanode and Pt Counter Electrode. The Ti plates (99.8% purity, Fuu Cherng Co. Ltd., Taiwan) were polished to remove metal oxides and other adhesive substances on the surfaces. The Ti plates and FTO (TEC-7, 10 Ω sq^{-1}, NSG America, Inc., NJ, U.S.A.) conducting glasses were first cleaned with a neutral cleaner and then washed sequentially with DI-water, acetone, and isopropanol.

The TiO_2 paste was prepared by first adding 72 mL of TTIP to 430 mL of aqueous solution with 0.1 M nitric acid. The colloid was heated at 85 °C for 8 h under constant stirring. The colloid was transferred to an autoclave (PARR 4540, U.S.A.) after it cooled to the room temperature, and afterward the colloid was heated at 240 °C for 12 h. The purpose of the heating is to make uniform growth of TiO_2 particles (ca. 20 nm). Two types of TiO_2 paste were fabricated by concentrating the as-prepared TiO_2 colloid 10 wt %. PEG (25 wt % with respect to the TiO_2) was added to the above solution to prepare the first type of TiO_2 paste, which was used to make a transparent layer, in which the target of adding PEG is to prevent the film from cracking and control the pore diameters during a drying process. On the other hand, the second type of TiO_2 paste for fabricating a scattering layer was made by incorporating 50 wt % of light scattering TiO_2 particles (PT-501A, 100 nm, Ya Chung Industrial Co. Ltd., Taiwan) with respect to the 20 nm TiO_2 particles in the first type of TiO_2 paste. This type of TiO_2 paste is used to reduce the light loss by back scattering. The conducting surface of the FTO glass was treated with a solution of TTIP in 2-methoxyethanol (weight ratio of 1:3) for obtaining a compact layer of TiO_2 to improve the mechanical contact between the conducting glass and the TiO_2 film and to isolate the conducting glass surface from the electrolyte. A 10 μm film of TiO_2 was coated by means of a doctor blade technique on the treated FTO glass, first with a transparent layer and then with a scattering layer. A portion of 0.4 × 0.4 cm^2 was selected for active area by scrapping the side portions. Each layer of the TiO_2 film was gradually heated to 450 °C in an oxygen atmosphere and was then sintered for 30 min at the same temperature. After it cooled to 80 °C, the TiO_2/FTO photoanode was immersed in a solution with 3 × 10^{-4} M of N719 sensitizer[31] in the mixed solvents of 50 vol % ACN and 50 vol % tBA at room temperature for 24 h.

The Ti plates with highly active surface area were prepared as follows. First, highly ordered TNTs were obtained on the surface of the Ti plates by anodization method.[32,33] The anodization was carried out at various voltages at the room temperature in an electrolyte containing 0.25 wt % NH_4F and 1.0 wt % H_2O in EG, for 1 h, to obtain the desired nanotube arrays. The anodized sheets were then dipped in DI-water and ultrasonically vibrated simultaneously to remove all the TNTs from their surface. The CEs were fabricated by loading Pt using a sputtering technique for 15 s on the above-obtained imprinted Ti plates, under a sputter current of 40 mA. The DSSC was fabricated by separating the photoanode and the CE using a 60 mm thick ionomer Surlyn (SX1170-25, Solaronix S.A., Aubonne, Switzerland). Afterward, the cell was sealed by heating, and then the electrolyte was injected between the electrodes by capillarity. A CE without TNT imprints on the substrate was used to prepare a reference DSSC.

Cell Assembly and Measurements. The DSSC was illuminated by a class A quality solar simulator (XES-301S, AM1.5G, San-Ei Electric Co., Ltd., Osaka, Japan), and the incident light intensity (100 mW cm^{-2}) was calibrated with a standard Si cell (PECSI01, Peccell Technologies, Inc.). The photoelectrochemical characteristics of the DSSCs were recorded with a potentiostat/galvanostat (PGSTAT 30, Autolab, Eco-Chemie, The Netherlands). Surface morphologies of the Ti plates were observed by scanning electron microscopy (SEM, Nova NanoSEM 230, FEI). The topography and surface roughness of the Ti plates were studied by atomic force microscopy (AFM, SEIKO E-sweep System, SII Nanotechnology Inc., Chiba, Japan), with a scanning probe microscope in tapping mode. CV was used to investigate active surface areas and catalytic abilities of the CEs. The CVs were obtained at a scan rate of 100 mV s^{-1}, using a three-electrode cell with a Pt-loaded TNT-imprinted Ti plate as the working electrode, a Pt foil as the auxiliary electrode, and an Ag/Ag^+ electrode as the reference electrode. The electrolyte solution contained 1.0 mM I_2, 10.0 mM LiI, and 0.1 M $LiClO_4$ in ACN or N_2-saturated 0.1 M H_2SO_4. A symmetrical sandwich-type cell is consisted of two identical electrodes each with an area of 1 cm^2 separated by a Surlyn spacer film of 60 μm thickness, and an electrolyte containing I^-/I_3^- was injected in between. The cell was used to investigate the electrocatalytic abilities of the CEs by EIS in the frequency range from 100 kHz to 10 mHz without applying any bias.[34] IPCE curves were obtained at short-circuit condition. The light source was a class A quality solar simulator (PEC-L11, AM1.5G, Peccell Technologies, Inc.); light was focused through a monochromator (Oriel Instrument, model 74100) onto the photovoltaic cell. The monochromator was moved in steps of 10 nm through the visible spectrum to generate the IPCE (λ) as defined in eq 1.

$$\mathrm{IPCE}(\lambda) = 1240\left(\frac{J_{SC}}{\lambda\varphi}\right) \quad (1)$$

DOI: 10.1021/am505025e
ACS Appl. Mater. Interfaces 2015, 7, 3910−3919

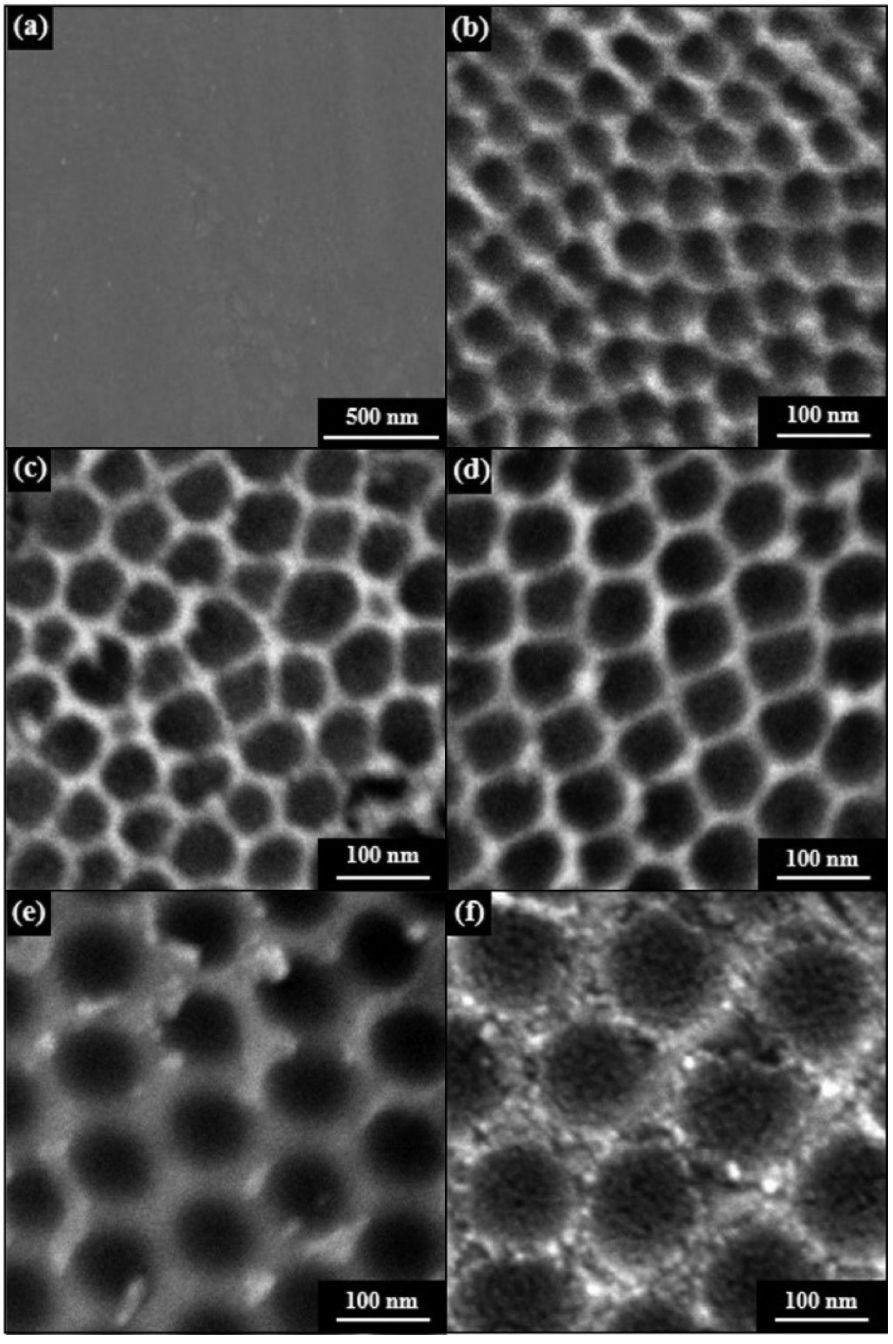

Figure 1. SEM images of (a) the Ti plate and TNT-imprinted Ti plates anodized at (b) 10, (c) 20, (d) 30, (e) 40, and (f) 50 V. The surfaces of the TNT-imprinted Ti plates are much rougher that of the bare Ti plate. The diameter of the circular TNT imprints increases with increasing anodization voltage, and the size of the imprints is the same as that of the original TNTs.

where λ is the wavelength, J_{SC} is short-circuit photocurrent density (mA cm^{-2}) recorded with a potentiostat/galvanostat, and φ is the incident radiative flux (W m^{-2}) measured with an optical detector (Oriel Instrument, model 71580) and a power meter (Oriel Instrument, model 70310).

RESULTS AND DISCUSSION

Surface Compositions and Morphologies of the Ti Plate and TiO_2 Nanotube-Imprinted Ti Plates. In our experiment, Ti plates were first anodized to get TNTs on their surfaces and then vibrated ultrasonically in the DI-water to detach the TNT. It is significant to confirm the complete detachment of the TNT from the anodized Ti plates in the preparation of TNT-imprinted Ti plates, since TNT is a kind of metal oxide that has relatively smaller conductivity compared to that of the Ti plate. Therefore, if the detachment of TNTs is not complete, some of the residual oxides remaining on the surface of the Ti plate would lead to the poor conductivity of the substrate and therefore may cause a decrease in the photovoltaic performance of the pertinent DSSC. XRD patterns were obtained to check the removal of TNT as shown in Figure S1 in the Supporting Information. Figure S1a,b shows the XRD patterns of non-sintered anodized Ti plates without and with ultrasonic vibrations in the DI-water, respectively. Amorphous TNT was expected to remain on the surface of the Ti plate in Figure S1a, while TNT was expected

DOI: 10.1021/am505025e
ACS Appl. Mater. Interfaces 2015, 7, 3910−3919

to be removed in Figure S1b. From XRD patterns, no significant difference was observed between Figure S1a and Figure S1b. Only peaks associated with Ti plate can be found in both cases. The most probable reason is that the TNT remained in the amorphous phase in absence of a sintering process, so regardless of whether the TNT is totally or partially detached from the surface of Ti plate after being subjected to ultrasonic vibrations, no significant difference can be observed. Therefore, sintering is an indispensable process for assuring the removal of TNT. Figure S1c,d shows the XRD patterns of anodized Ti plates that have undergone a sintering process without and with ultrasonic vibrations in the DI-water, respectively. The XRD pattern shows a peak corresponding to the anatase phase of TiO_2 at (101) for Figure S1c, indicating the formation of crystalline TNT, while no peak associated with the anatase phase of TiO_2 can be observed in Figure S1d. The results confirm the complete removal of TNT on the surface of Ti plate after the ultrasonic vibrations. Otherwise, the peak associated with the anatase phase of TiO_2 would be found in Figure S1d.

Surface morphologies of the Ti plate and the TNT-imprinted Ti plates obtained at different anodization voltages were examined in Figure 1. Figure 1a shows a flat Ti plate with almost no grains on the surface, while coarse surfaces are observed on the contrary for the TNT-imprinted Ti plates anodized at 10, 20, 30, 40, and 50 V in Figure 1b,c,d,e,f, respectively. Continuous circular TNT imprints can be obtained for all of the TNT-imprinted Ti plates, and the corresponding diameter increases with increasing anodization voltage. The diameter of the circular imprints is the same as that of the TNT existing before applying ultrasonic vibration on the anodized Ti plates. It is well-known that the self-organized TNT formed by anodization of Ti plates involves pore initiation, pore propagation, and growth steps. The formation of a thin TiO_2 layer occurred at the beginning of anodization, and then a high field effect induced the pore initiation across the TiO_2 layer by causing a localized breakdown phenomenon. Pore growth originated at the pits formed by chemical dissolution process. Continuous repeated field-assisted dissolution and chemical dissolution resulted in hollow-like cylindrical oxide that would develop into the nanotubular structure. The effect of anodization voltage on the diameter of TNT is related to the number of pits formed during the early stage of the anodization process. The Ti plates anodized at high voltage would suffer from severe electric field dissolution forming more pits at an early stage of anodization. These pits will be etched to form larger pores. As growth of the pores dominates, the resulting diameter of TNT becomes larger when anodization is performed at higher voltage.[35] The average diameters of TNT imprints on the Ti plates anodized at 10, 20, 30, 40, and 50 V estimated from the SEM images are 44, 53, 61, 74, and 105 nm, respectively. On the other hand, the surface roughness of the Ti plate and TNT-imprinted Ti plates with different anodized voltages were examined from the AFM images, as shown in Figure 2. It is observed that the surface morphology of the Ti plate is very smooth when compared to those of the TNT-imprinted Ti plates shown in Figure 2a, while increasing depth was found with increasing anodization voltage for the TNT-imprinted Ti plates. Average root-mean-square (RMS) roughness values and depth were obtained for the TNT-imprinted Ti plates with 10, 20, 30, 40, and 50 V as the anodization voltage, as shown in Figure 2b,c,d,e,f, respectively, and listed in Table 1. At higher anodization

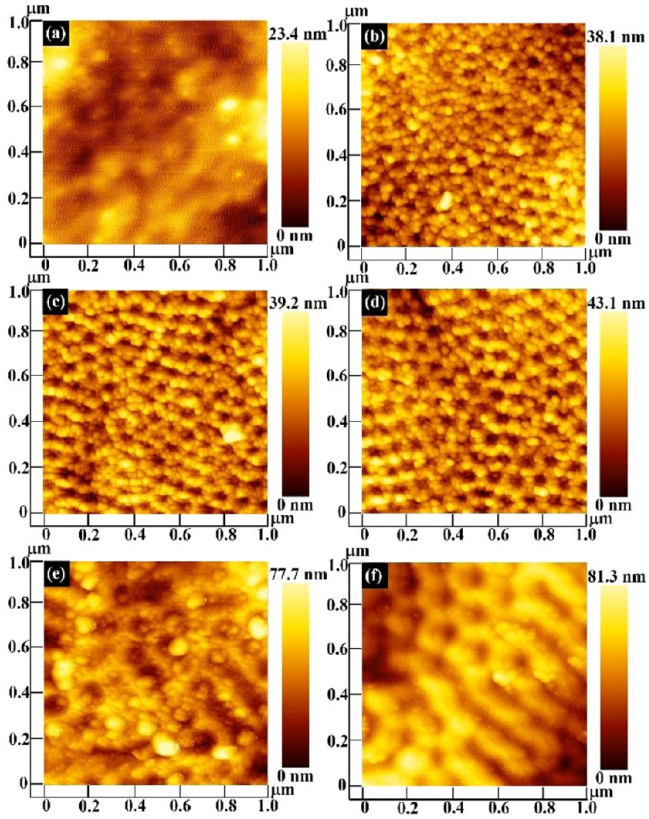

Figure 2. AFM images of (a) the Ti plate and TNT-imprinted Ti plates anodized with (b) 10, (c) 20, (d) 30, (e) 40, and (f) 50 V. The depth of the circular TNT imprints increases with increasing anodization voltage.

Table 1. Average Root-Mean-Square (RMS) Roughness and Depth Values of the Pt-Loaded Ti Plate and Pt-Loaded TNT-Imprinted Ti Plates Obtained from AFM Images; Total Measured Charges and the Estimated Values of Active Surface Areas of the Pt-Loaded Ti Plate and Pt-Loaded TNT-Imprinted Ti Plates Obtained from CV in Figure S2

anodization voltage (V)	RMS (nm)	average depth (nm)	$Q_{measured}$ (10^{-5} C)	A_{act} (cm^2)
0	4.0		8.1	4.0
10	6.0	21.1	9.7	4.6
20	6.3	24.3	11.8	5.6
30	6.8	26.7	22.1	10.6
40	12.4	29.1	19.7	9.4
50	14.5	32.5	17.2	8.2

voltage, the electric field-induced dissolution at the barrier layer occurred at a much faster deepening rate, thus forming longer nanotubes, which resulted in deeper imprints on the Ti plates after removal of TNTs.[35] Moreover, to investigate the uniformity of the TNT-imprinted Ti plates, a 3 × 10 cm^2 Ti plate was anodized, and the TNTs on the surface were removed to obtain the TNT-imprinted Ti plate, as shown in Figure 3. The bottom image shows the as-anodized Ti plate, which was taken before removing TNT on its surface, while the top image represents the TNT-imprinted Ti plate, which was first anodized and then treated by the ultrasonic vibration in DI-water to remove all the TNT on its surface. High uniformity and the feasibility for large-scale production of the TNT-imprinted Ti plate are demonstrated by comparing the three

DOI: 10.1021/am505025e
ACS Appl. Mater. Interfaces 2015, 7, 3910−3919

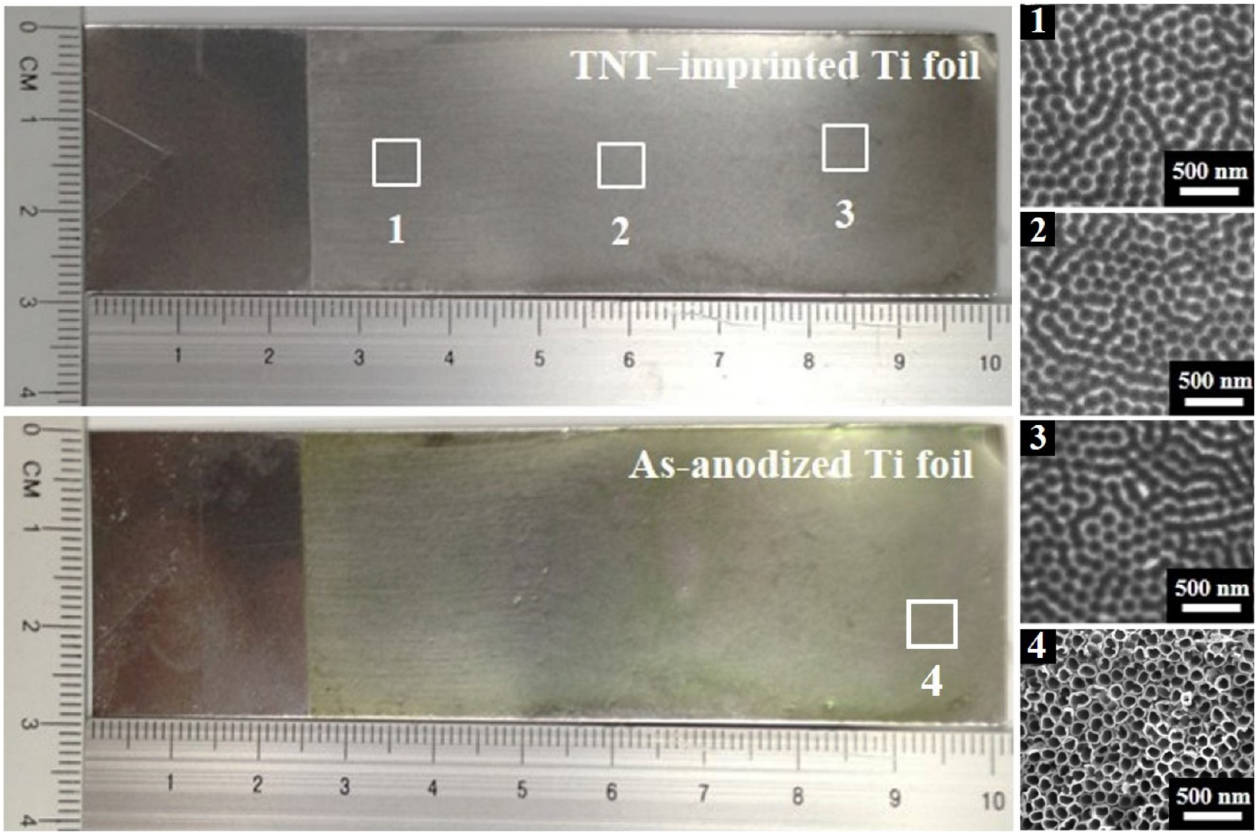

Figure 3. Photos of a 3 × 10 cm^2 large-scale as-anodized Ti plate and a TNT-imprinted Ti plate. The SEM images labeled 1, 2, and 3 were taken from the selected areas of the TNT-imprinted Ti plate to investigate the uniformity of the imprints, and the SEM image labeled 4 was obtained from the selected area of the as-anodized Ti plate. The high uniformity and large-scale production flexibility of the TNT-imprinted Ti plate are confirmed in this figure.

SEM images taken from various parts of the TNT-imprinted Ti plate. Also, an SEM image of the as-anodized Ti plate was also obtained in Figure 3 and labeled 4 as a reference.

Active Surface Areas of the Pt-Loaded Ti Plate and Pt-Loaded TiO_2 Nanotube-Imprinted Ti Plates. CV analysis was used to estimate the active surface areas (A_{act}) of the Pt-loaded Ti plate and Pt-loaded TNT-imprinted Ti plates.[36] The CVs were obtained in a 0.1 M aqueous solution of N_2-saturated H_2SO_4 at a scan rate of 100 mV s^{-1} as shown in Figure S2 in the Supporting Information. The A_{act} of Ti plates was estimated by first obtaining the total charge under the hydrogen-desorption region by integrating the currents under the curves of CV within the range from 0 to 0.4 V (vs Ag/AgCl/saturated KCl), followed by subtracting the corresponding double layer charge from the total charge, and a value of 210 μC cm^{-2} ($Q_{monolayer}$) for the monolayer of hydrogen adsorbed on the polycrystalline platinum was used as the conversion factor in the calculation to obtain the value of A_{act}.[37] The total charges and the estimated values of A_{act} are summarized in Table 1. The largest value of A_{act} (10.6 cm^2) was obtained for the Pt-loaded TNT-imprinted Ti plate anodized at 30 V (Pt-imprinted Ti plate (30 V)). As observed from SEM and AFM images, respectively, shown in Figures 1 and 2, the diameter and the depth of TNT imprints increase along with the increasing anodization voltage. Increases in the diameter lead to decreases in the number of TNT imprints per unit area, resulting in smaller active surface area, while increases in the depth cause higher active surface area reversely. Therefore, the highest active surface area of the TNT-imprinted Ti plate was obtained for the case with a middle anodization voltage, that is, 30 V. The best catalytic ability for the redox reaction of I^-/I_3^- was also expected in this case. To further illustrate the changes in diameter, depth, and therefore the active surface area, the schematic top and cross-sectional views of the TNT-imprinted Ti plates are shown in Scheme S1. After examination for the surface properties of the Ti plates with and without TNT imprints modification, the cell performance of the DSSCs based on these Ti plates was further investigated.

Photovoltaic Performance and Incident Photon-to-Current Conversion Efficiency Spectra of DSSCs. Figure 4a shows the photocurrent density–voltage (J–V) curves of the DSSCs with Pt-loaded Ti plate and Pt-loaded TNT-imprinted Ti plates as the CEs, and the corresponding photovoltaic parameters are listed in Table 2. For the comparison of the Pt-loaded Ti plate and Pt-loaded TNT-imprinted Ti plates based DSSCs, higher η were obtained for the latter cases, due to their larger active surface areas for Pt deposition, leading to better electrocatalytic abilities for I^-/I_3^- redox reaction, as illustrated in Scheme 1. On the other hand, among the DSSCs with Pt-loaded TNT-imprinted Ti plates as the CEs, the highest η and short-circuit current density (J_{SC}) of 9.35% and 18.67 mA cm^{-2}, respectively, was achieved for the cell with 30 V as the anodization voltage. As observed in Table 2, the values of J_{SC} and η increase with increasing anodization voltage until the voltage reaches 30 V, and then they decrease with further increases in the anodization voltage. The initial increases in J_{SC} and η values for the cases with the anodization voltage ranged from 10 to 30 V are attributed to the deeper imprints of TNT

DOI: 10.1021/am505025e
ACS Appl. Mater. Interfaces 2015, 7, 3910–3919

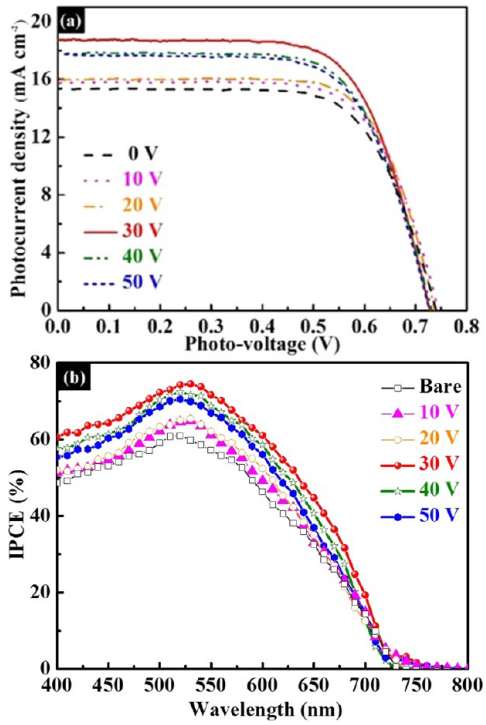

Figure 4. (a) $J-V$ curves obtained at 100 mW cm^{-2} light intensity and (b) IPCE spectra of the DSSCs with the Pt-loaded Ti plate (0 V) and Pt-loaded TNT-imprinted Ti plates. The better performance was obtained for the DSSC with the Pt-loaded TNT-imprinted Ti plates as its counter electrode due to the better catalytic ability for I^-/I_3^- redox reaction obtained by the higher active surface area of the CE substrates.

caused by larger anodization voltage to induce larger driving force for F^- ions etching the Ti plate in the presence of electrolyte containing NH_4F, and thereby higher active surface area as well as better catalytic ability can be obtained with higher anodization voltage. On the contrary, the following decreases in J_{SC} and η values with the increasing anodization voltage for the cases with the anodization voltage ranged from 30 to 50 V are caused by increases in the diameter of TNT imprints on Ti plates, leading to decreases in the number of TNT imprints per unit area, and thereby to decreases in the active surface area as well as the corresponding catalytic ability. The IPCE spectra of the DSSCs with the Pt-loaded Ti plate and Pt-loaded TNT-imprinted Ti plates are shown in Figure 4b. IPCE is defined as the number of electrons in the external circuit produced at a given wavelength divided by the number of incident photons. The maximum IPCE values are at the wavelength of 530 nm, which coincides with the absorption maximum wavelength of N719 dye. The maximum IPCE value is 75.0% for the DSSC with Pt-loaded TNT-imprinted Ti plates (30 V) and is considerably higher than that of the cell with Pt-loaded Ti plate (55.3%). Moreover, the DSSC with Pt-loaded Ti plate (30 V) shows the highest IPCE values among the cases with Pt-loaded TNT-imprinted Ti plates as the CEs over the whole spectral region. Normally, IPCE is the combination result of the light harvesting, the light injection, and the electron collection efficiencies.[33] The light-harvesting efficiency is primarily dependent on the absorption spectrum of the dye on the TiO_2 photoanode, and the light-injection efficiency is dependent upon the electronic coupling of the dye to TiO_2 and lowest unoccupied molecular orbital (LUMO) energy of the dye relative to the band of electron accepting orbitals of TiO_2. Since the substrate of the CE is Ti plate, which allows no light to transmit through it, the transmittance of the CE should be zero no matter whether the Ti plate has an imprinted treatment or not, indicating all the light was reflected and absorbed. The reflection spectra of the bare Ti plate and the imprinted Ti plate were shown in Figure S3 in the Supporting Information. A smaller reflection of 39% at 530 nm was obtained for the imprinted Ti plate, due to its rougher surface compared to that of the imprinted Ti plate, which shows a higher reflection of 48%. Although the reflection is different between the bare Ti plate and the imprinted Ti plate, the influence is negligible. Since light reflected by the substrate of the CE, that is, the Ti plate, will be absorbed by the electrolyte before arriving at the photoanode, the slight difference between the reflection of 48% and 39%, respectively, for the bare Ti plate and the imprinted Ti plate will be even smaller.[38] Therefore, the differences on the light-harvesting and light-injection efficiencies between the DSSCs with bare Ti plate and imprinted Ti plate as their CE substrates could be neglected. We assume the light-harvesting and light-injection efficiencies are the same for all of the DSSCs since their photoanodes are prepared under the same condition and since the incident lights are similar. Hence, the improvement on the IPCE for the DSSC with imprinted Ti plate as the CE substrate is mainly due to the enhanced electron collection efficiency, which depends on the competition between the recombination and the transport of electrons to the photoanode.[33] The enhanced electron collection efficiency can be attributed to the better catalytic ability of the CE, which can enhance the redox reaction in the electrolyte and reduce the charge recombination.

Electrocatalytic Abilities of the Pt-Loaded Ti Plate and Pt-Loaded TiO_2 Nanotube-Imprinted Ti Plates for the Triiodide Reduction. To evaluate the electrocatalytic abilities of the counter electrodes, CV, EIS, and Tafel polarization

Table 2. Photovoltaic Parameters of the DSSCs (three cells were made under each condition) with the Pt-Loaded Ti Plate and Pt-Loaded TNT-Imprinted Ti Plates, Obtained at 100 mW cm^{-2} Light Intensity; Cathodic Peak Current Densities (I_{pc}) and Charger Transfer Resistances (R_{ct}) of the Pt-Loaded Ti Plate and Pt-Loaded TNT-Imprinted Ti Plates

anodized voltage (V)	V_{OC} (V)	J_{SC} (mA cm^{-2})	J_{SC}[a] (mA cm^{-2})	FF	η (%)	I_{pc} (mA cm^{-2})	R_{ct} (Ω cm^2)
0	0.73 ± 0.01	15.43 ± 0.22	15.64	0.68 ± 0.02	7.70 ± 0.10	1.26	19.89
10	0.75 ± 0.01	15.83 ± 0.24	15.97	0.68 ± 0.01	8.13 ± 0.07	1.28	10.35
20	0.74 ± 0.02	15.93 ± 0.19	16.32	0.70 ± 0.01	8.29 ± 0.23	1.33	9.14
30	0.73 ± 0.01	18.67 ± 0.13	18.93	0.69 ± 0.02	9.35 ± 0.12	1.53	1.14
40	0.73 ± 0.01	17.83 ± 0.28	17.97	0.68 ± 0.02	8.83 ± 0.16	1.44	2.85
50	0.73 ± 0.01	17.67 ± 0.11	17.74	0.68 ± 0.01	8.62 ± 0.11	1.40	4.94

[a]The J_{SC} values are obtained by integrating the IPCE curves shown in Figure 4b.

DOI: 10.1021/am505025e
ACS Appl. Mater. Interfaces 2015, 7, 3910−3919

Scheme 1. Illustration of the I^-/I_3^- Redox Reaction Catalyzed by Pt Occurring on (a) the Pt-Loaded Flat Ti Plate and (b) the Pt-Loaded TNT-Imprinted Ti Plate

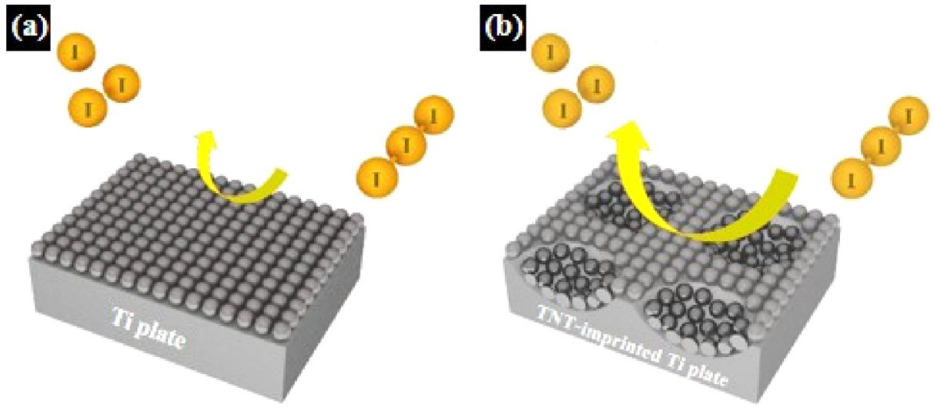

curves were applied. Cyclic voltammetry with a three-electrode cell is one of the promising electrochemical analysis methods to identify the electrocatalytic ability of the electrode for catalyzing the redox couple mediator.[39−42] According to the CV curve, the potential of the redox reaction and the related current density can be obtained, and other useful information for evaluating the catalytic ability of the electrodes can be extracted, too. For example, the electrocatalytic active surface area and the reaction activity can be evaluated by using the peak current density and the peak separation, respectively. In addition, the Tafel polarization curve with a two-electrode cell system was used to get the exchange current density and related charge transfer resistance at the region with the bias close to zero for evaluating the catalytic ability of the CEs.

Figure 5a shows overlaid CVs recorded for the Pt-loaded Ti plate and Pt-loaded TNT-imprinted Ti plates, which play the role of the CE in DSSCs. In a DSSC, the photoexcited electrons from the dye are injected into the TiO_2 conduction band. The oxidized dye is then reduced by the I^- ions in the electrolyte, and the resulting I_3^- ions are reduced at the CE. The redox reactions at the photoanode and the CE are shown in eq 2 and eq 3, respectively.

$$3I^- \rightarrow I_3^- + 2e^- \quad (2)$$

$$I_3^- + 2e^- \rightarrow 3I^- \quad (3)$$

The electrocatalytic ability of a CE can be affected by the electrochemical active surface area of its substrate and the electrocatalytic activity of the material on the CE. The cathodic peak current density (I_{pc}) at a more negative potential (ca. −0.3 V vs Ag/Ag^+)[43] can serve as a measure of the electrocatalytic ability for the I^-/I_3^- redox reaction at the CE. The I_{pc} values for the Pt-loaded Ti plate and Pt-loaded TNT-imprinted Ti plates are summarized in Table 2.

All of the Pt-loaded TNT-imprinted Ti plates show higher I_{pc} than that of the Pt-loaded Ti plate, while the Pt-imprinted Ti plate (30 V) shows the highest I_{pc} value of 1.53 mA cm^{-2}, suggesting its best electrocatalytic ability for the I^-/I_3^- redox reaction. The I_{pc} values show the same tendency as those of the corresponding active surface areas, indicating the only reason for the better electrocatalytic abilities of the Pt-loaded TNT-imprinted Ti plates is the higher active surface areas for Pt deposition owing to the TNT imprints on the substrates. The catalytic activity of a CE depends also on the charge transfer resistance (R_{ct}) at the CE/electrolyte interface. To evaluate the values of the R_{ct} for the CEs with the Pt-loaded Ti plate and Pt-loaded TNT-imprinted Ti plates, EIS measurements were carried out using a symmetrical cell with two identical CEs, that is, two identical Pt-loaded Ti plates or Pt-loaded TNT-

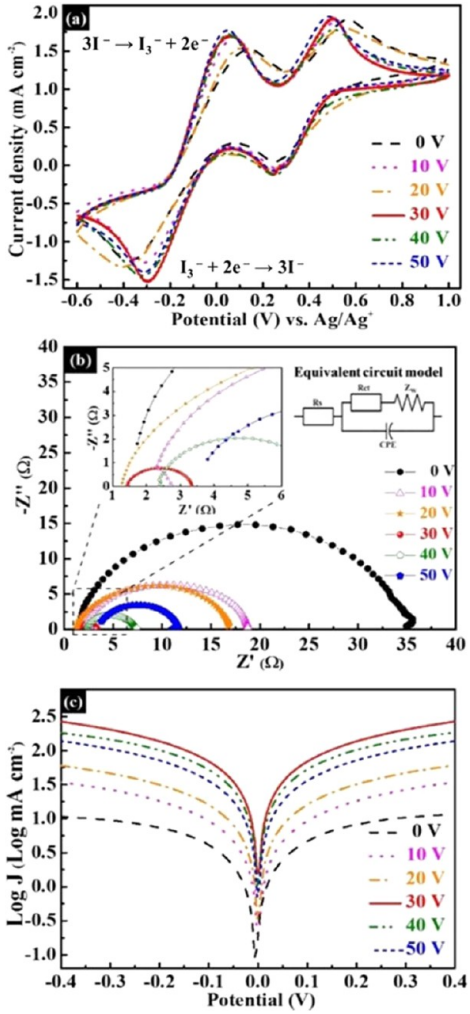

Figure 5. (a) CVs of the Pt-loaded Ti plate (0 V) and Pt-loaded TNT-imprinted Ti plates for I^-/I_3^- redox reaction in an ACN solution with 10.0 mM LiI, 1.0 mM I_2, and 0.1 M $LiClO_4$. (b) Nyquist plots. (inset) Portion of Nyquist plots at high frequencies. (c) Tafel polarization curves of the Pt-loaded Ti plate (0 V) and Pt-loaded TNT-imprinted Ti plates for I^-/I_3^- redox reaction obtained using symmetrical cells with two identical electrodes.

DOI: 10.1021/am505025e
ACS Appl. Mater. Interfaces 2015, 7, 3910−3919

imprinted Ti plates. Figure 5b shows typical Nyquist plots of the CEs. The impedance at high frequency where the phase is zero is represented by the series resistance (R_S), the semicircle on the left side represents the R_{ct} at the lectrode/electrolyte interface and the corresponding double layer capacitance (CPE), and the other semicircle on the right side represents the Warburg diffusion impedance (Z_W) for the redox couple in the electrolyte. The inset on the left side of Figure 5b shows the portion of Nyquist plots for the CEs at high frequencies. The diameter of the semicircle represents the charge transfer resistance. Table 2 also lists the values of R_{ct} for the Pt-loaded Ti plate and Pt-loaded TNT-imprinted Ti plates. It is clearly observed that the R_{ct} value of the Pt-loaded Ti plate is much larger than those of the Pt-loaded TNT-imprinted Ti plates, suggesting the worst catalytic activity of the Pt-loaded Ti plate for the I^-/I_3^- redox reaction.[41] On the other hand, the smallest value of R_{ct} (1.14 Ω cm^2) can be found for the Pt-loaded imprinted-Ti plate (30 V), which further confirms its best electrocatalytic ability for the I^-/I_3^- redox reaction in the electrolyte. In fact, the R_{ct} value obtained from the EIS measurement depends on the counter electrode and the electrolyte. Assuming that the effect of electrolyte is negligible, a preliminary literature survey suggests that the R_{ct} with a value smaller than 3 Ω cm^2 would serve as an index for a good counter electrode.[40,44−47] The best case of the counter electrode in this study (R_{ct} = 1.14 Ω cm^2) meets this criterion. To further investigate the catalytic activities, Tafel polarization curves were obtained for the Pt-loaded Ti plate and TNT-imprinted Ti plates using a symmetrical cell with two identical CEs, as shown in Figure 5c, presenting logarithmic current density (log I) as a function of voltage (V). The exchange current density (J_0) related to the catalytic activity of the electrode can be obtained at the small overpotential region. In this region, the cathodic branch for the curve of Pt-loaded TNT-imprinted Ti plate shows a larger slope as compared to that of the Pt-loaded Ti plate, indicating a high J_0 on the surface of the former case according to the Tafel equation and therefore the better catalytic ability for the reduction of I_3^- to I^-.[48] Increases in the anodization voltage from 10 to 30 V cause increases in the J_0 value, and further increases in the anodization voltage lead to decreasing value of J_0. Therefore, the highest J_0 value was obtained for the Pt-loaded imprinted Ti plate (30 V). This tendency is consistent with those observed in the peak current densities in the CV, and ultimately with the J_{SC} and η values of the corresponding DSSCs. In addition, R_{ct} varies inversely with J_0 according to eq 4.

$$J_0 = \frac{RT}{nFR_{ct}} \tag{4}$$

where R is the gas constant, T is the absolute temperature, F is the Faraday constant, n is the number of electrons involved in the reduction of I_3^- at the electrode, and R_{ct} is the charge transfer resistance. In this study, the relation between J_0 and R_{ct} is consistent with this equation.[49] Although the charge transfer resistance at the interface of the counter electrode and the electrolyte, R_{ct}, is different, the difference may be relatively small when compared with the total internal resistance. Therefore, it is very likely that the value of R_{ct} would not influence the FF value to a large extent in our case, as supported by some reports in the literature that there is no clear correlation between the values of FF and R_{ct}.[50−54] In fact, some reports indicated that the FF value is influenced by the R_{ct} value, that is, the larger the R_{ct}, the smaller the FF.[55−60] Since there are so many factors to influence the FF, our study suggests no obvious relationship between the values of FF and R_{ct}, which is in good agreement with the previous literature.[50−54]

This study reports on the preparation of Ti plates with TNT imprints and their application in DSSCs as the substrate for CEs. The DSSC with a flexible Pt-loaded TNT-imprinted Ti plate as its CE shows a high η value of 9.35%. The combination of this flexible CE with a flexible photoanode is expected to become a full-fledged flexible DSSC. Lightweight and flexible DSSCs have advantages of easy transportation and roll-to-roll production, which makes them cost-effective.

CONCLUSIONS

Ti plates with high active surface area were prepared through anodization to obtain TNTs on the surface, followed by the removal of TNTs; consequently, only the TNT imprints retained on the surface of Ti plates. TNT imprints with different diameters and profundities were obtained by applying different anodization voltages. XRD analysis demonstrated the existence and removal of TNTs. SEM images show continuous circular TNT imprints on the surface of all the TNT-imprinted Ti plates. The increasing diameter and depth of the TNT imprints on the Ti plate with increasing anodization voltage were observed from SEM and AFM images, respectively. The highest value of the active surface area (10.6 cm^2) was obtained for the Pt-loaded imprinted Ti plate (30 V). All the DSSCs with Pt-loaded TNT-imprinted Ti plates show higher J_{SC} and η than those of the DSSC with Pt-loaded Ti plate, due to the better catalytic abilities for the reduction of I_3^- to I^- for the former cases. The higher catalytic ability of Pt-sputtered TNT-imprinted Ti plates is verified through CV, electrochemical impedance spectra, and Tafel plots. A high η value of 9.35% was obtained for the DSSC with the Pt-loaded imprinted Ti plate (30 V) with its highest IPCE value of 75.0%.

ASSOCIATED CONTENT

Supporting Information

Top and cross-sectional views of TNT-imprinted Ti plates, XRD patterns of the anodized Ti plates, CVs of Pt-sputtered Ti plate and TNT-imprinted plates, reflection spectra of pristine Ti plate and the TNT-imprinted Ti plate. This material is available free of charge via the Internet at http://pubs.acs.org.

AUTHOR INFORMATION

Corresponding Authors

*E-mail: lylin@ntut.edu.tw. (L.Y.L.)
*E-mail: vittal.dr@gmail.com. (V.R.)
*E-mail: kcho@ntu.edu.tw. (K.C.H.)

Author Contributions

$^{\phi}$These authors contributed equally. The manuscript was written through contributions of all authors. All authors have given approval to the final version of the manuscript.

Notes

The authors declare no competing financial interest.

ACKNOWLEDGMENTS

This work was supported in part by the Ministry of Science and Technology (MOST) of Taiwan. Some of the instruments used in this study were made available through the financial support of the Academia Sinica, Taipei, Taiwan. This work was

DOI: 10.1021/am505025e
ACS Appl. Mater. Interfaces 2015, 7, 3910−3919

supported in part by the National Taiwan University (NTU) and the National Taipei University of Technology (NTUT).

REFERENCES

(1) Liu, R.; Yang, W. D.; Wu, J. F.; Qiang, L. S. Fabrication of the Effective Counter Electrode for Dye-Sensitized Solar Cells. *Adv. Mater. Res.* **2011**, *197*, 1143−1146.
(2) Lee, K. S.; Lee, H. K.; Wang, D. H.; Park, N. G.; Lee, J. Y.; Park, O. O.; Park, J. H. Dye-sensitized Solar Cells with Pt- and TCO-free Counter Electrodes. *Chem. Commun.* **2010**, *46*, 4505−4507.
(3) Wang, G.; Lin, R.; Lin, Y.; Li, X.; Zhou, X.; Xiao, X. A Novel High-performance Counter Electrode for Dye-sensitized Solar Cells. *Electrochim. Acta* **2005**, *50*, 5546−5552.
(4) Murakami, T. N.; Grätzel, M. Counter Electrodes for DSC: Application of Functional Materials as Catalysts. *Inorg. Chim. Acta* **2008**, *361*, 572−580.
(5) Han, W.; Bando, Y.; Kurashima, K.; Sato, T. Boron-doped Carbon Nanotubes Prepared through a Substitution Reaction. *Chem. Phys. Lett.* **1999**, *299*, 368−373.
(6) Wang, J.; Lin, Z. Dye-sensitized TiO_2 Nanotube Solar Cells with Markedly Enhanced Performance via Rational Surface Engineering. *Chem. Mater.* **2010**, *22*, 579−584.
(7) Calogero, G.; Calandra, P.; Irrera, A.; Sinopoli, A.; Citro, I.; Di Marco, G. A New Type of Transparent and Low Cost Counter-electrode Based on Platinum Nanoparticles for Dye-sensitized Solar Cells. *Energy Environ. Sci.* **2011**, *4*, 1838−1844.
(8) Fang, X.; Ma, T.; Guan, G.; Akiyama, M.; Kida, T.; Abe, E. Effect of the Thickness of the Pt Film Coated on a Counter Electrode on the Performance of a Dye-sensitized Solar Cell. *J. Electroanal. Chem.* **2004**, *570*, 257−263.
(9) Huang, K. C.; Wang, Y. C.; Dong, R. X.; Tsai, W. C.; Tsai, K. W.; Wang, C. C.; Chen, Y. H.; Vittal, R.; Lin, J. J.; Ho, K. C. A High Performance Dye-sensitized Solar Cell with a Novel Nanocomposite Film of PtNP/MWCNT on the Counter Electrode. *J. Mater. Chem.* **2010**, *20*, 4067−4073.
(10) Kim, S.; Nah, Y.; Noh, Y.; Jo, J.; Kim, D. Electrodeposited Pt for Cost-efficient and Flexible Dye-sensitized Solar Cells. *Electrochim. Acta* **2006**, *51*, 3814−3819.
(11) Yang, C. C.; Zhang, H. Q.; Zheng, Y. R. DSSC with a Novel Pt Counter Electrodes using Pulsed Electroplating Techniques. *Curr. Appl. Phys.* **2011**, *11*, S147−S153.
(12) Tsekouras, G.; Mozer, A. J.; Wallace, G. G. Enhanced Performance of Dye Sensitized Solar Cells Utilizing Platinum Electrodeposit Counter Electrodes. *J. Electrochem. Soc.* **2008**, *155*, K124−K128.
(13) Yoon, C.; Rvittal; Lee, J.; Chae, W.; Kim, K. Enhanced Performance of a Dye-sensitized Solar Cell with an Electrodeposited-platinum Counter Electrode. *Electrochim. Acta* **2008**, *53*, 2890−2896.
(14) Fang, X.; Ma, T.; Guan, G.; Akiyama, M.; Abe, E. Performances Characteristics of Dye-sensitized Solar Cells Based on Counter Electrodes with Pt Films of Different Thickness. *J. Photochem. Photobiol., A* **2004**, *164*, 179−182.
(15) Vomiero, A.; Galstyan, V.; Braga, A.; Concina, I.; Brisotto, M.; Bontempi, E.; Sberveglieri, G. Flexible Dye Sensitized Solar Cells using TiO_2 Nanotubes. *Energy Environ. Sci.* **2011**, *4*, 3408−3413.
(16) Toivola, M.; Ahlskog, F.; Lund, P. Industrial Sheet Metals for Nanocrystalline Dye-sensitized Solar Cell Structures. *Sol. Energy Mater. Sol. Cells* **2006**, *90*, 2881−2893.
(17) Chang, H.; Chen, T. L.; Huang, K. D.; Chien, S. H.; Hung, K. C. Fabrication of Highly Efficient Flexible Dye-sensitized Solar Cells. *J. Alloys Compd.* **2010**, *504*, S435−S438.
(18) Mathew, X.; Thompson, G. W.; Singh, V. P.; McClure, J. C.; Velumani, S.; Mathews, N. R.; Sebastian, P. J. Development of CdTe Thin Films on Flexible Substrates–A Review. *Sol. Energy. Mater. Sol. Cells* **2003**, *76*, 293−303.
(19) Huang, X.; Yin, Z.; Wu, S.; Qi, X.; He, Q.; Zhang, Q.; Yan, Q.; Boey, F.; Zhang, H. Graphene-based Materials: Synthesis, Characterization, Properties, and Applications. *Small* **2011**, *7*, 1876−1902.
(20) Miettunen, K.; Asghar, I.; Ruan, X.; Halme, J.; Saukkonen, T.; Lund, P. Stabilization of Metal Counter Electrodes for Dye Solar Cells. *J. Electroanal. Chem.* **2011**, *653*, 93−99.
(21) Wang, G.; Lin, Y. Novel Counter Electrodes Based on NiP-plated Glass and Ti Plate Substrate for Dye-sensitized Solar Cells. *J. Mater. Sci.* **2007**, *42*, 5281−5285.
(22) Yin, C.; Zhu, S.; Yao, F.; Gu, J.; Zhang, W.; Chen, Z.; Zhang, D. Biomimetic Fabrication of WO_3 for Water Splitting under Visible Light with High Performance. *J. Nanopart. Res.* **2013**, *15*, 1−11.
(23) Liu, Q.; Chen, Q.; Bai, J.; Li, J.; Li, J.; Zhou, B. Enhanced Photoelectrocatalytic Performance of Nanoporous WO_3 Photoanode by Modification of Cobalt−phosphate (Co−Pi) Catalyst. *J. Solid State Electrochem.* **2013**, *18*, 157−161.
(24) Fu, N. Q.; Fang, Y. Y.; Duan, Y. D.; Zhou, X. W.; Xiao, X. R.; Lin, Y. High-Performance Plastic Platinized Counter Electrode via Photoplatinization Technique for Flexible Dye-Sensitized Solar Cells. *ACS Nano* **2012**, *6*, 9596−9605.
(25) Kim, D. J.; Koh, J. K.; Lee, C. S.; Kim, J. H. Mesh-Shaped Nanopatterning of Pt Counter Electrodes for Dye-Sensitized Solar Cells with Enhanced Light Harvesting. *Adv. Energy Mater.* **2014**, DOI: 10.1002/aenm.201400414.
(26) Hasin, P.; Alpuche Aviles, M. A.; Li, Y.; Wu, Y. Mesoporous Nb-doped TiO_2 as Pt Support for Counter Electrode in Dye-sensitized Solar Cells. *J. Phys. Chem. C* **2009**, *113*, 7456−7460.
(27) Yang, C.; Wang, Z.; Lin, T.; Yin, H.; Lu, X.; Wan, D.; Xu, T.; Zheng, C.; Lin, J.; Huang, F.; Xie, X.; Jiang, M. Core-shell Nanostructured "black" Rutile Titania as Excellent Catalyst for Hydrogen Production Enhanced by Sulfur Doping. *J. Am. Chem. Soc.* **2013**, *135*, 17831−17838.
(28) Ishihara, H.; Kannarpady, G. K.; Khedir, K. R.; Woo, J.; Trigwell, S.; Biris, A. S. A Novel Tungsten Trioxide (WO_3)/ITO Porous Nanocomposite for Enhanced Photo-catalytic Water Splitting. *Phys. Chem. Chem. Phys.* **2011**, *13*, 19553−19560.
(29) Yun, H. G.; Jun, Y.; Kim, J.; Bae, B. S.; Kang, M. G. Effect of Increased Surface Area of Stainless Steel Substrates on the Efficiency of Dye-sensitized Solar Cells. *Appl. Phys. Lett.* **2008**, *93*, 133311.
(30) Yun, H. G.; Bae, B. S.; Kang, M. G. A Simple and Highly Efficient Method for Surface Treatment of Ti Substrates for Use in Dye-Sensitized Solar Cells. *Adv. Energy Mater.* **2011**, *1*, 337−342.
(31) Nazeeruddin, M. K.; Splivallo, R.; Liska, P.; Comte, P.; Grätzel, M. A Swift Dye Uptake Procedure for Dye Sensitized Solar Cells. *Chem. Commun.* **2003**, 1456−1457.
(32) Fukishima, A.; Honda, K. Electrochemical Photolysis of Water at a Semiconductor Electrode. *Nature* **1972**, *238*, 37−38.
(33) Barnes, P. R. F.; Anderson, A. Y.; Koops, S. E.; Durrant, J. R.; Regan, B. C. O. Electron Injection Efficiency and Diffusion Length in Dye-sensitized Solar Cells Derived from Incident Photon Conversion Efficiency Measurements. *J. Phys. Chem. C* **2009**, *113*, 1126−1136.
(34) Yeh, M. H.; Lin, L. Y.; Su, J. S.; Leu, Y. A.; Vittal, R.; Sun, C. L.; Ho, K. C. Nanocomposite Graphene/Pt Electrocatalyst as Economical Counter Electrode for Dye-Sensitized Solar Cells. *ChemElectroChem* **2014**, *1*, 416−425.
(35) Lai, C. W.; Sreekantan, S. Fabrication of WO_3 Nanostructures by Anodization Method for Visible-light Driven Water Splitting and Photodegradation of Methyl Orange. *Mater. Sci. Semicond. Process.* **2013**, *16*, 303−310.
(36) Radovic Hrapovic, Z.; Jerkiewicz, G. The Temperature Dependence of the Cyclic-voltammetry Response for the Pt(110) Electrode in Aqueous H_2SO_4 Solution. *J. Electroanal. Chem.* **2001**, *499*, 61−66.
(37) Sheppard, S. A.; Campbell, S. A.; Smith, J. R.; Lloyd, G. W.; Walsh, F. C.; Ralph, T. R. Electrochemical and Microscopic Characterisation of Platinum-coated Perfluorosulfonic Acid (Nafion 117) Materials. *Analyst* **1998**, *123*, 1923−1929.
(38) Lin, L. Y.; Lee, C. P.; Vittal, R.; Ho, K. C. Improving the Durability of Dye-sensitized Solar Cells through Back Illumination. *J. Power Sources* **2011**, *196*, 1671−1676.
(39) Yang, Z.; Liu, M.; Zhang, C.; Tjiu, W. W.; Liu, T.; Peng, H. Carbon Nanotubes Bridged with Graphene Nanoribbons and Their

DOI: 10.1021/am505025e
ACS Appl. Mater. Interfaces 2015, 7, 3910−3919

Use in High-Efficiency Dye-Sensitized Solar Cells. *Angew. Chem., Int. Ed.* **2013**, *52*, 1−5.
(40) Tai, S. Y.; Liu, C. J.; Chou, S. W.; Chien, F. S. S.; Lin, J. Y.; Lin, T. W. Few-layer MoS_2 Nanosheets Coated onto Multi-walled Carbon Nanotubes as a Low-cost and Highly Electrocatalytic Counter Electrode for Dye-sensitized Solar Cells. *J. Mater. Chem.* **2012**, *22*, 24753−24759.
(41) Wu, M.; Lin, X.; Hagfeldt, A.; Ma, T. A Novel Catalyst of WO_2 Nanorod for the Counter Electrode of Dye-sensitized Solar Cells. *Chem. Commun.* **2011**, *47*, 4535−4537.
(42) Lin, L. Y.; Nien, P. C.; Lee, C. P.; Tsai, K. W.; Yeh, M. H.; Vittal, R.; Ho, K. C. Low-Temperature Flexible Photoanode and Net-Like Pt Counter Electrode for Improving the Performance of Dye-Sensitized Solar Cells. *J. Phys. Chem. C* **2010**, *114*, 21808−21815.
(43) Kubo, W.; Kambe, S.; Nakade, S.; Kitamura, T.; Hanabusa, K.; Wada, Y.; Yanagida, S. Photocurrent-determining Processes in Quasi-solid-state Dye-sensitized Solar Cells using Ionic Gel Electrolytes. *J. Phys. Chem. B* **2003**, *107*, 4374−4381.
(44) Tang, Z.; Wu, J.; Zheng, M.; Tang, Q.; Liu, Q.; Lin, J.; Wang, J. High Efficient PANI/Pt Nanofiber Counter Electrode used in Dye-sensitized Solar Cell. *RSC Adv.* **2012**, *2*, 4062−4064.
(45) Wu, M.; Bai, J.; Wang, Y.; Wang, A.; Lin, X.; Wang, L.; Shen, Y.; Wang, Z.; Hagfeldt, A.; Ma, T. High-performance Phosphide/Carbon Counter Electrode for Both Iodide and Organic Redox Couples in Dye-sensitized Solar Cells. *J. Mater. Chem.* **2012**, *22*, 11121−11127.
(46) Sudhagar, P.; Nagarajan, S.; Lee, Y. G.; Song, D.; Son, T.; Cho, W.; Heo, M.; Lee, K.; Won, J.; Kang, Y. S. Synergistic Catalytic Effect of a Composite (CoS/PEDOT:PSS) Counter Electrode on Triiodide Reduction in Dye-sensitized Solar Cells. *ACS Appl. Mater. Interfaces* **2011**, *3*, 1838−1843.
(47) Li, G. R.; Wang, F.; Song, J.; Xiong, F. Y.; Gao, X. P. TiN-conductive Carbon Black Composite as Counter Electrode for Dye-sensitized Solar Cells. *Electrochim. Acta* **2012**, *65*, 216−220.
(48) Jiang, Q. W.; Li, G. R.; Gao, X. P. Highly Ordered TiN Nanotube Arrays as Counter Electrodes for Dye-sensitized Solar Cells. *Chem. Commun.* **2009**, 6720−6722.
(49) Bard, A. J.; Faulkner, L. R. *Electrochemical Methods: Fundamentals and Applications,* 2nd ed.; John Wiley & Sons, Inc.: New York, 2001.
(50) Liao, Y.; Pan, K.; Wang, L.; Pan, Q.; Zhou, W.; Miao, X.; Jiang, B.; Tian, C.; Tian, G.; Wang, G.; Fu, H. Facile Synthesis of High-crystallinity Graphitic Carbon/Fe_3C Nanocomposites as Counter Electrodes for High-efficiency Dye-sensitized Solar Cells. *ACS Appl. Mater. Interfaces* **2013**, *5*, 3663−3670.
(51) Chen, H.; Kou, D.; Chang, Z.; Zhou, W.; Zhou, Z.; Wu, S. Effect of Crystallization of $Cu_2ZnSnS_xSe_{4-x}$ Counter Electrode on the Performance for Efficient Dye-sensitized Solar Cells. *ACS Appl. Mater. Interfaces* **2014**, *6*, 20664−20669.
(52) He, J.; Lee, L. T.; Yang, S.; Li, Q.; Xiao, X.; Chen, T. Printable Highly Catalytic Pt- and TCO-free Counter Electrode for Dye-sensitized Solar Cells. *ACS Appl. Mater. Interfaces* **2014**, *6*, 2224−2229.
(53) Zhao, W.; Lin, T.; Sun, S.; Bi, H.; Chen, P.; Wan, D.; Huang, F. Oriented Single-crystalline Nickel Sulfide Nanorod Arrays: "two-in-one" Counter Electrodes for Dye-sensitized Solar Cells. *J. Mater. Chem. A* **2013**, *1*, 194−198.
(54) Song, M. Y.; Chaudhari, K. N.; Park, J.; Yang, D. S.; Kim, J. H.; Kim, M. S.; Lim, K.; Ko, J.; Yu, J. S. High Efficient Pt Counter Electrode Prepared by Homogeneous Deposition Method for Dye-sensitized Solar Cell. *Appl. Energy* **2012**, *100*, 132−137.
(55) Dao, V. D.; Choi, H. S. Dry Plasma Synthesis of a MWNT-Pt Nanohybrid as an Efficient and Low-cost Counter Electrode Material for Dye-sensitized Solar Cells. *Chem. Commun.* **2013**, *49*, 8910−8912.
(56) Yun, S.; Wu, M.; Wang, Y.; Shi, J.; Lin, X.; Hagfeldt, A.; Ma, T. Pt-like Behavior of High-performance Counter Electrodes Prepared from Binary Tantalum Compounds Showing High Electrocatalytic Activity for Dye-sensitized Solar Cells. *ChemSusChem* **2013**, *6*, 411−416.
(57) Ke, W.; Fang, G.; Tao, H.; Qin, P.; Wang, J.; Lei, H.; Liu, Q.; Zhao, X. In Situ Synthesis of NiS Nanowall Networks on Ni Foam as a TCO-free Counter Electrode for Dye-sensitized Solar Cells. *ACS Appl. Mater. Interfaces* **2014**, *6*, 5525−5530.
(58) Tai, S. Y.; Liu, C. J.; Chou, S. W.; Chien, F. S. S.; Lin, J. Y.; Lin, T. W. Few-layer MoS_2 Nanosheets Coated onto Multi-walled Carbon Nanotubes as a Low-cost and Highly Electrocatalytic Counter Electrode for Dye-sensitized Solar Cells. *J. Mater. Chem.* **2012**, *22*, 24753−24759.
(59) Lan, J. L.; Wan, C. C.; Wei, T. C.; Hsu, W. C.; Peng, C.; Chang, Y. H.; Chen, C. M. Improvement of Photovoltaic Performance of Dye-sensitized Solar Cell by Post Heat Treatment of Polymer-capped Nano-platinum Counter Electrode. *Int. J. Electrochem. Sci.* **2011**, *6*, 1230−1236.
(60) Wang, Y. C.; Wang, D. Y.; Jiang, Y. T.; Chen, H. A.; Chen, C. C.; Ho, K. C.; Chou, H. L.; Chen, C. W. FeS_2 Nanocrystal Ink as a Catalytic Electrode for Dye-sensitized Solar Cells. *Angew. Chem., Int. Ed. Engl.* **2013**, *52*, 6694−6698.

DOI: 10.1021/am505025e
ACS Appl. Mater. Interfaces 2015, 7, 3910−3919